


IDK1 is a rat monoclonal antibody against hypoglycosylated bone sialoprotein with application as biomarker and therapeutic agent in breast cancer skeletal metastasis

Michael Zepp¹, Marineta Kovacheva¹, Munkhtsetseg Altankhuyag², Gabriela Westphal², Irina Berger², Katharina S Gather³, Heidegard Hilbig³, Jochen Neuhaus⁴, Gertrud M Hänsch⁵, Franz P Armbruster⁶ and Martin R Berger^{1*} 

¹Toxicology and Chemotherapy Unit, German Cancer Research Center, Heidelberg, Germany

²Institute of Pathology, Klinikum Kassel, Kassel, Germany

³Institute of Anatomy, University of Leipzig, Leipzig, Germany

⁴Urology Clinic, University Hospital, Leipzig, Germany

⁵Institute of Immunology, University Hospital Heidelberg, Heidelberg, Germany

⁶Immundiagnostik AG, Bensheim, Germany

*Correspondence to: Martin R Berger, Toxicology and Chemotherapy Unit, German Cancer Research Center, Im Neuenheimer Feld 581, 69120 Heidelberg, Germany. E-mail: m.berger@dkfz.de

Abstract

Changes in glycosylation are salient features of cancer cells. Here, we report on the diagnostic and therapeutic properties of IDK1, an antibody against tumour associated, hypoglycosylated bone sialoprotein (hypo-BSP). The affinity of the rat monoclonal antibody IDK1 for hypo-BSP, as determined by microscale thermophoresis, was three orders of magnitude higher than for mature BSP, whereas the mouse monoclonal antibody used had similar affinity for both BSP forms. IDK1 showed no activity against the proliferation or migration of normal or cancer cells growing *in vitro*. *In vivo*, however, IDK1 caused dose-dependent regression of soft tissue and skeletal lesions in nude rats harbouring human MDA-MB-231 cells. At optimal dose, 80% of the treated rats showed complete remission of all tumour lesions. Analysis of BSP expression *in vitro* by fluorescence-activated cell sorting (FACS) and immunocytochemistry showed basal levels of this protein, which were visible only in a fraction of these cells. Cells of the metastatic cell lines MDA-MB-231 and PC-3 were more often positive for hypo-BSP. In addition, there was co-expression of both forms in some cells, but almost no co-localization; rather, hypo-BSP was present in the nucleus, and mature BSP was detected extra-cellularly. Normal osteoblasts and osteoclasts were negative for hypo-BSP. Breast cancer tissue, however, showed strong expression of mature BSP, which was present intra-cellularly as well as in vesicles outside cells. Hypo-BSP was present mainly in lesions from skeletal sites, thus explaining the antineoplastic activity of IDK1, which was high in lesions growing in the vicinity of the skeleton but low in lesions growing subcutaneously. Finally, hypo-BSP was detected in specimens from breast cancer patients, with a significantly greater intensity in skeletal metastases as compared to the respective primary cancers. In conclusion, IDK-1 is an antibody with diagnostic and therapeutic applications in skeletal metastases of breast cancer.

Keywords: hypoglycosylated bone sialoprotein; biomarker; immunohistochemical method; immunocytochemistry

Received 3 June 2017; Revised 9 November 2017; Accepted 11 November 2017

Conflict of interest statement: F P Armbruster is CEO of Immundiagnostik AG. All other authors state no conflict of interest.

Introduction

Protein glycosylation is a major posttranslational modification in mammalian cells. Aberrant glycosylation is frequently observed in various diseases, including cancer. The altered glycosylation pattern may result in different protein folding and biological functions [1]. The glycosylation status of a cell is dynamic and

alters upon oncogenesis, whereby cancer cells, compared to their healthy counterparts, express more branched N-glycans, higher levels of fucosylated and sialylated glycans and a truncated O-glycan phenotype. This abundant cancer glycosylation profile is currently considered a hallmark of cancer [2]. It is

assumed that tumour-associated O-glycans not only support tumour growth, but are a major factor underlying the development of an immune suppressive tumour microenvironment and actively contribute to immune evasion [1]. In line with this pathophysiology, a shortened O-glycan phenotype was identified for tumour-associated bone sialoprotein (BSP) [3] and termed hypoglycosylated BSP (hypo-BSP).

BSP is a secreted, sialic acid-rich, phosphorylated glycoprotein with an apparent molecular mass of 70–80 kDa [3]. It belongs to the small integrin-binding ligand N-linked glycoprotein (SIBLING) family of proteins and is part of the major non-collagenous organic matrix fractions in bone [4]. Physiologically, BSP is synthesized by osteoblasts, osteoclasts, osteocytes, and chondrocytes [5] and contains an Arg-Gly-Asp (RGD) sequence located in the C-terminus of the protein, which is a common recognition site for integrins [6,7] such as $\alpha_v\beta_3$ and $\alpha_v\beta_5$. BSP acts as a promoter for the initial formation of mineral crystals in bone, cementum, and dentine and as an early marker of osteogenic differentiation. In addition to its physiological roles, BSP has been associated with prognosis of breast cancer patients, since elevated serum levels were a marker of subsequent bone metastasis and highly related to poor survival [8,9]. BSP was found in primary malignancies such as breast [8,10], prostate [11], and thyroid cancers [12]. Specifically, the BSP-mediated interaction between tumour cells and bone tissue was suspected to participate in the pathogenesis of bone metastasis [5,8,13–15]. BSP enhances migration of cells through matrices by bridging MMP-2 to $\alpha_v\beta_3$ -integrin [16]. Beyond that, it is assumed that the secretion of BSP from tumour cells provides a selective advantage for their survival. Here, the RGD motif of BSP binds to the cell surface receptor $\alpha_v\beta_3$ -integrin and then to complement factor H (cfH), which protects tumour cells from the lytic activity of the complement system [15].

Based on the observed altered O-glycan phenotype of tumour-associated BSP, a set of antibodies was developed that recognize a BSP form which is hypoglycosylated at Thr 125. Here, we report on diagnostic and therapeutic properties of these antibodies against hypo-BSP in experimental systems and in human pathology samples.

Materials and methods

Cell culture

The non-tumorigenic immortalized human mammary epithelial cell line MCF-10 was cultured in Mammary

Epithelial Growth Medium (PromoCell, Heidelberg, Germany). The other cell lines (human breast cancer cell lines MDA-MB-231^{GFP/Luc} and MCF-7, human prostate cancer cell line PC3, human osteosarcoma cell line SaOS-2, human ovarian cancer cell line SK-OV3) were cultured in Roswell Park Memorial Institute (RPMI)-1640 medium (Invitrogen, Karlsruhe, Germany) supplemented with 10% fetal bovine serum (FBS), 2 mM L-glutamine, 100 U/ml penicillin and 100 µg/ml streptomycin (Invitrogen, Germany). The cells were maintained in cell culture flasks (TPP, Switzerland) in an incubator (37°C, humidified atmosphere, 5% CO₂). They were propagated 2–3 times per week to keep them in logarithmic growth.

Isolation of monocytes and differentiation to osteoclasts

Monocytes were isolated from peripheral blood as described previously [17] and in supplementary material, Supplementary materials and methods. Cells were stimulated with either RANKL or interleukin-8 and differentiation was monitored microscopically.

Osteoblast primary culture

Primary osteoblasts were isolated from spongiosa as described in supplementary material, Supplementary materials and methods.

Monoclonal antibodies

Monoclonal antibodies against BSP were generated as described in supplementary material, Supplementary materials and methods. In brief, the monoclonal rat anti-BSP antibody IDK-1 was raised against the hypoglycosylated epitope TGLAA (aa125–130), IDK-2 was raised against pentameric TGLAA, and IDK-3 was raised against an epitope of the main and carboxy-terminal domains of BSP (aa84–318).

Cell proliferation assay (MTT)

The 3-(4,5-dimethylthiazol-2-yl)-2,5-diphenyltetrazolium-bromide (MTT) assay was used as described previously [18] and in supplementary material, Supplementary materials and methods to assess an anti-proliferative effect on tumour cells.

Migration assay

Cell migration in response to antibody exposure was determined as described previously [18] and in supplementary material, Supplementary materials and methods.

Cytofluorometry

Expression of mature BSP and hypo-BSP was tested as published previously [19] and described in supplementary material, Supplementary materials and methods.

Immunoblotting

Immunoblotting was performed as published previously [20] and described in supplementary material, Supplementary materials and methods.

Affinity of antibodies

Microscale thermophoresis was used to determine the binding affinity of antibodies to BSP forms. Experiments were performed according to the protocol (Monolith NT™ Protein Labelling Kit) and as described in supplementary material, Supplementary materials and methods. The dissociation constant (KD) describing the binding affinity of antibodies was calculated using the software NTAnalysis 1.5.41 from NanoTemper® Technologies GmbH.

Animals and husbandry

Male nude rats [Rowett nude rat (RNU) strain] were obtained at an age of 5–6 weeks from commercial sources and kept as described previously [21].

Ethics statement

All animal experiments were carried out in accordance with the recommendations in the Guide for the Management Ordinance of Laboratory Animals of the Society of Laboratory Animals (GV-SOLAS, Germany). The protocols were approved by the Regierungspräsidium Karlsruhe, Germany. All surgeries were performed under anaesthesia, and all efforts were made to minimize suffering.

Tumour cell inoculation

MDA-MB-231^{GFP/Luc} tumour cells were injected into the femoral artery of nude rats as described previously [21] and in supplementary material, Supplementary materials and methods.

Bioluminescence imaging, magnetic resonance imaging, and computed tomography

The appearance and development of bone metastases were monitored by imaging methods, as described previously [21,22].

Immunocytochemistry

Experiments were performed in Lab Tec™ chamber slides™. The cells were fixed in paraformaldehyde (4%, in PBS) and subjected to immunostaining [4',6-diamidino-2-phenylindole (DAPI) plus one or two antibodies] as described in supplementary material, Supplementary materials and methods. In addition to primary antibodies (mouse monoclonal A4232.2 against mature BSP; rat monoclonal IDK-1 against hypo-BSP; rabbit polyclonal antibody against human complement cfH, and rabbit polyclonal antibody against human integrin $\alpha_V\beta_3$) the corresponding tetramethylrhodamine (TRITC)- or fluorescein isothiocyanate (FITC)-conjugated secondary antibodies were used. After staining with antibodies, cell preparations were counterstained with DAPI (Serva), diluted 1:1000 and cover-slipped. Visualization and image processing are described in detail in supplementary material, Supplementary materials and methods.

Immunohistochemistry

Immunohistochemistry was performed in general as described previously [23]; details of the newly established procedures with the anti-BSP antibodies are described in supplementary material, Supplementary materials and methods.

Evaluation procedure

The results were evaluated by a pathologist (IB) for lesion severity, intensity of staining, and percentage of positive cells after inspection of all fields in the tissue sections. For evaluation of the ductal structures, sections were scanned at low ($\times 50$) magnification. Analysis and semi-quantitative evaluation were performed using an Axioplan-2 microscope (Carl Zeiss, Jena, Germany). Semi-quantitative evaluation was based on quantity of tumour cells (scores 1–4) and colour intensity (scores 1–3), the results of which were multiplied to yield results ranging from 1 to 12.

Patient selection and ethics

Samples from 11 human primary breast tumours and their corresponding skeletal metastases were obtained by random selection from the archives of the Institute of Pathology, Kassel, Germany. Informed consent of these patients had been obtained at the time of deposition, ranging from 2012 to 2015.

Statistics

Experimental results were recorded and depicted by their mean and corresponding standard deviation. For

proliferation and migration assays, all results were given in percent of the untreated control.

For animal experiments, the bioluminescence imaging (BLI) data were evaluated using the program 'Living Image' (PerkinElmer GmbH, Germany) and the intensity of the emitted photons flux was given by the respective units (photons/s/cm²/steradian). This program also converted the numerical values into a pseudo-colour graphic for visualization of the tumour burden.

Differences between control and treated groups were assessed by the distribution-independent Kruskal-Wallis test, which compares rank sums from the respective experimental groups. *P* values ≤ 0.05 were considered significant. Differences in ratios were evaluated by Pearson's chi-squared test (χ^2).

Results

Affinity of BSP-antibodies

The affinity of BSP-antibodies to mature and hypo-BSP was determined by micro-scale thermophoresis. Based on this method, a control antibody (monoclonal mouse antibody against parathyroid hormone) did not show any affinity towards mature or hypo-BSP. The mouse monoclonal antibody directed against the C-terminal part of BSP (aa84–318) showed good affinity for mature BSP ($KD = 3.5 \times 10^{-7}$ M) and similar affinity for hypo-BSP ($KD = 4.2 \times 10^{-7}$ M). The rat monoclonal antibody IDK-1, raised against the hypoglycosylated peptide TGLAA (aa125–130 of BSP) showed moderate affinity ($KD = 2.7 \times 10^{-7}$ M) for hypo-BSP, but negligible affinity for mature BSP ($KD = 8.6 \times 10^{-3}$ M). The rat monoclonal antibody IDK-2, showed distinct affinity for hypo-BSP ($KD = 3.2 \times 10^{-9}$ M) and no affinity for mature BSP. Finally, the rat monoclonal antibody IDK-3, showed negligible affinity for hypo-BSP ($KD = 7.9 \times 10^{-3}$ M) and a similar affinity for mature BSP ($KD = 4.9 \times 10^{-4}$ M). Diagrams showing the corresponding normalized fluorescence versus concentration data are shown in supplementary material, Figure S1.

Effect of BSP-antibodies on proliferation and migration

For testing whether antibodies directed against hypo-BSP inhibit basic cellular properties, MDA-MB-231^{GFP/Luc} breast cancer cells were exposed for 1–3 days to IDK-1, IDK-2, or IDK-3 concentrations ranging from 100 to 900 µg/ml to determine effects on proliferation, and for 1–4 days to antibody concentrations

ranging from 25 to 400 µg/ml, for effects on migration. Under these conditions, neither the proliferation nor the migration of MDA-MB-231^{GFP/Luc} cells was inhibited to a discernible degree (supplementary material, Table S1). The same result was obtained when FBS was used without heat inactivation (data not shown).

Subsequently, the anti-proliferative effect of antibody IDK-1 was tested in PC3 (human prostate carcinoma) cells and primary human osteoblasts. Similar to MDA-MB-231 cells, exposure to a concentration of 200 µg/ml for 2–4 days did not change the proliferation of PC3 cells, or that of osteoclasts (similar conditions; data not shown).

To confirm these results by a second method, the percentage of apoptotic and necrotic cells in response to antibody IDK-1 was determined in MDA-MB-231 cells by flow cytometry. Following double staining with Annexin V and propidium iodide, there was no significant increase in apoptotic or necrotic cells following exposure to IDK-1 (concentration 5–100 µg/ml, 4–24 h). In contrast, exposure to formalin as necrosis inducing agent caused an increase in necrotic cells from 13% to 81% within 60 min (supplementary material, Figure S2A).

Effect of anti-BSP antibodies *in vivo*

Growth of soft tissue and skeletal lesions was monitored by bioluminescence and magnetic imaging as well as computed tomography (CT). A representative control rat is shown in supplementary material, Figure S3. The three monoclonal rat antibodies against hypo-BSP were investigated in rats for their effect against MDA-MB-231^{GFP/Luc}-induced skeletal lesions as well as the surrounding soft tumour tissue (see Table 1). Initially, treatment started 2 weeks after tumour cell inoculation via the femoral artery of a rat's hind leg. The antibody treatment was administered twice weekly for 6 weeks and caused differential types of response. Either there was a time-dependent continuous increase in soft tumour growth, as indicated by increasing light emission, as for untreated controls (Figure 1A–C), which was termed 'progressive disease'. This response corresponded to an increasing mass of soft tumour tissue concomitantly with growing osteolytic lesions (Figure 1D, CT-reconstruction), which caused premature euthanasia of the animals for ethical reasons.

Alternatively, the tumour growth was halted, as shown by the respective light emission, which did not increase further (Figure 1E–G) and this type of response was termed 'no change'. Finally, the light emission of the tumour died out (Figure 1I–K) and this indicated a 'complete remission' of both soft

Table 1. Experimental design and results of treating nude rats implanted with MDA-MB-231^{Luci/RFP} breast cancer cells with antibodies directed against hypoglycosylated BSP

Group	Rat no. N (%)	Treatment	Start of treatment after tumour inoculation	Progressive disease N (%)	Stable disease/partial remission N (%)	Complete remission N (%)	Death during treatment period N (%)
I a	10 (100)	Control*	2 weeks	9 (90)	0 (0)	1 (10)	0 (0)
I b	10 (100)	IDK-1; 5 mg/kg [†]	2 weeks	1 (10)	1 (10)	8 (80)	0 (0)
II a	10 (100)	Control*	2 weeks	10 (100)	0 (0)	0 (0)	0 (0)
II b	10 (100)	IDK-2; 5 mg/kg [†]	2 weeks	0 (0)	1 (10)	6 (60)	3 (30)
III a	10 (100)	Control*	2 weeks	10 (100)	0 (0)	0 (0)	0 (0)
III b	10 (100)	IDK-3; 5 mg/kg [†]	2 weeks	6 (60)	3 (30)	1 (10)	0 (0)
IV a	10 (100)	Control*	4 weeks	10 (100)	0 (0)	0 (0)	0 (0)
IV b	10 (100)	IDK-1; 5 mg/kg [†]	4 weeks	0 (0)	4 (40)	6 (60)	0 (0)
V a	10 (100)	Control*	4 weeks	10 (100)	0 (0)	0 (0)	0 (0)
V b	10 (100)	IDK-2; 5 mg/kg [†]	4 weeks	0 (0)	1 (10)	5 (50)	4 (40)
VI a	8 (100)	Control*	2 weeks	8 (100)	0 (0)	0 (0)	0 (0)
VI b	8 (100)	IDK-1; 5 mg/kg [†]	2 weeks	0 (0)	3 (37.5)	5 (62.5)	0 (0)
VI c	8 (100)	IDK-1; 2.5 mg/kg [‡]	2 weeks	2 (25)	3 (37.5)	3 (37.5)	0 (0)
VII a	6 (100)	Control*	2 weeks	6 (100)	0 (0)	0 (0)	0 (0)
VII b	6 (100)	Pretreatment [§]	2 weeks	1 (16.7)	0 (0)	5 (83.3)	0 (0)
VII c	6 (100)	Pretreatment [§]	2 weeks	2 (33.3)	1 (16.7)	3 (50)	0 (0)
VII d	6 (100)	Pretreatment [¶]	2 weeks	1 (16.7)	0 (0)	5 (83.3)	0 (0)

*Control animals received 0.9% NaCl injections.

[†]Dose was administered twice weekly for 6 weeks.

[‡]Tumour cells were pre-incubated with IDK-1 (50 µg/ml) for 3 days before inoculation.

[§]Animals were pre-treated with IDK-1 (2 × 5 mg/kg) 1 week before tumour cell inoculation.

[¶]Tumour cells were pre-incubated and the animals were pre-treated with IDK-1 (combination of [‡] and [§]).

tumour tissue and osteolytic lesions as confirmed by CT (Figure 1L) and subsequent histology (supplementary material, Figure S4). The observed changes in tumour growth were measured by BLI and are shown in Figure 1M.

Administration of IDK 1–3 at 5 mg/kg concentrations started 2 weeks after tumour cell inoculation and was continued twice weekly for 6 weeks (Table 1, groups I–III). Remarkably, IDK-1 caused complete remission in 8 of 10 rats, and no change or progressive disease in 1 of 10 rats, respectively. IDK-3 was distinctly less effective, as shown by complete remission in 1 of 10 rats, no change in 3 of 10 rats, and progressive disease in 6 of 10 rats. IDK-2 was also less effective than IDK-1, but more toxic than the other two antibodies as shown by complete remission in 6 of 10 rats and death related to IDK-2 toxicity in 3 of 10 animals. In comparison, there was progressive tumour growth in 29 of 30 control rats, corresponding to a spontaneous remission rate of 3%. Because of insufficient efficacy, IDK-3 was omitted from further analysis.

In subsequent experiments, the time after tumour inoculation until onset of treatment was prolonged from 2 to 4 weeks (Table 1, groups IV and V). As a result, 6 of 10 rats treated with IDK-1 showed complete remission, and 4 of 10 animals showed partial remission or no change. This contrasted to 5 complete and 1 partial remissions out of 10 rats following IDK-2, as well as 4 of 10 animals dying due to toxicity within the treatment period. In these experiments, all 20 control rats showed progressive disease.

After excluding IDK-2 from subsequent experiments for its toxicity, IDK-1 was investigated for its dose-effect relationship (Table 1, groups VI a–c). In fact, administration of a dose reduced by 50% (2.5 mg/kg twice weekly for 6 weeks) was associated with complete remission in 3 of 8 rats, no change in 3 of 8 rats, and progressive disease in 2 of 8 rats. Again, 8 of 8 control rats showed progressive disease.

Finally, neither pre-treatment of MDA-MB-231^{GFP/Luc} cells *in vitro*, nor administration of IDK-1 to rats prior to tumour cell inoculation, nor the combination

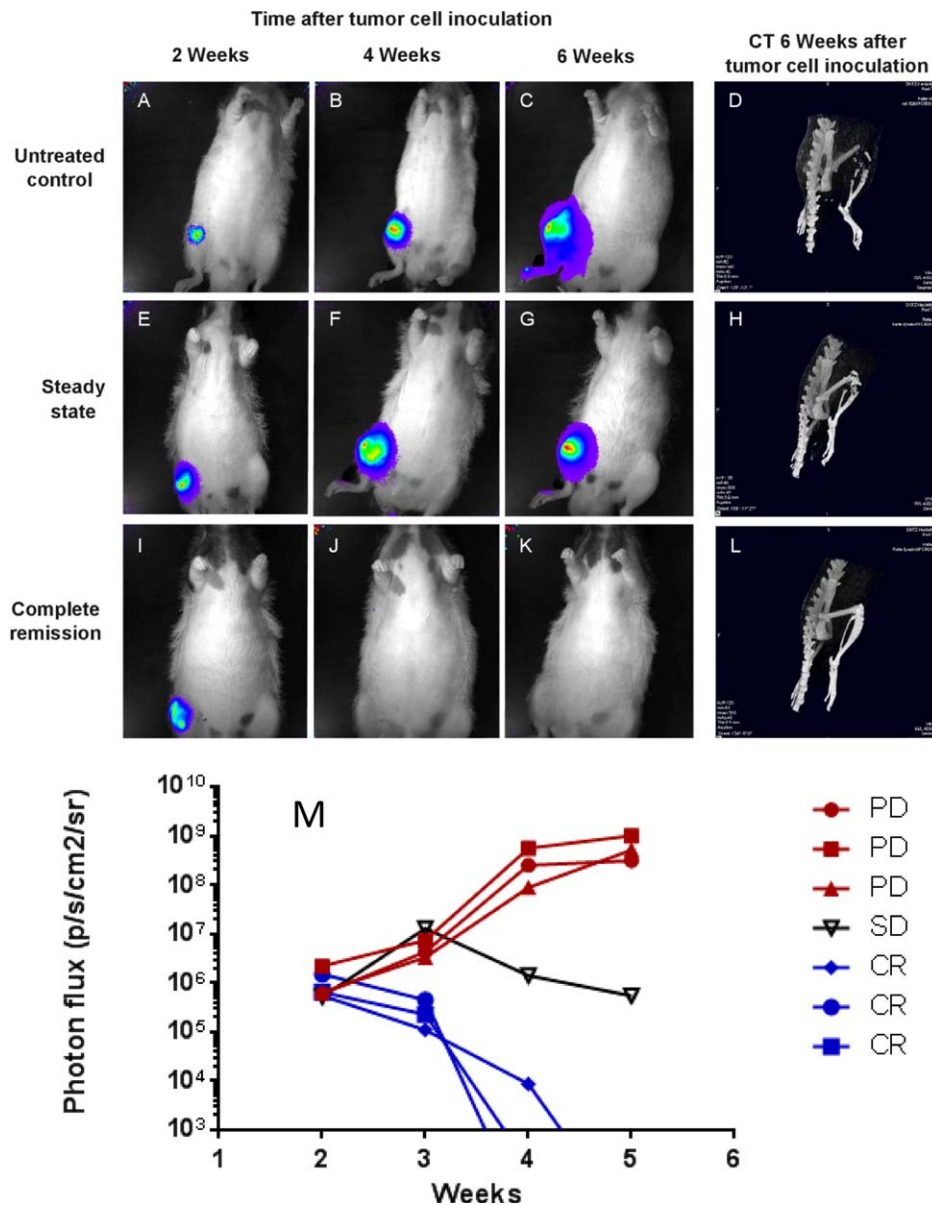


Figure 1. BLI and CT for soft tumour and skeletal lesions in control and antibody-treated rats inoculated with MDA-MB-231 breast cancer cells. Nude rats were implanted with MDA-MB-231^{Luc/RFP} cells via the femoral artery of their right hind leg. BLI and CT were used for monitoring soft tumour size and extent of skeletal lesions. For BLI, rats were injected with luciferin and the resulting light emission from tumour cells marked with the luciferase gene was recorded. Control rats (A–C) showed a steady increase in tumour size as indicated by light emission (red: most intense, blue: least intense). Antibody-treated rats showed either a steady tumour size (E–G) or a complete remission, indicated by the disappearance of light signals (I–K). At the end of the observation period, the status of soft tumour lesions was correlated with that of skeletal lesions as determined by CT (D, H, L). A graph (M) showing experimental time in weeks versus intensity of photon emission (p/s/cm²/sr) compares representative animals with progressive disease (PD, red) with stable disease (SD, black) and rats showing complete remission (CR, blue).

of these two types of ‘additive’ therapy increased the rate of complete remissions to ratios higher than those observed when starting the IDK-1 treatment at 2 weeks following tumour inoculation (80%).

Flow cytometry detection of BSP-forms in tumour cell lines

The presence of mature and hypo-BSP was analysed with the mouse monoclonal antibody (A4232.2) and the rat monoclonal antibody IDK1 (both from

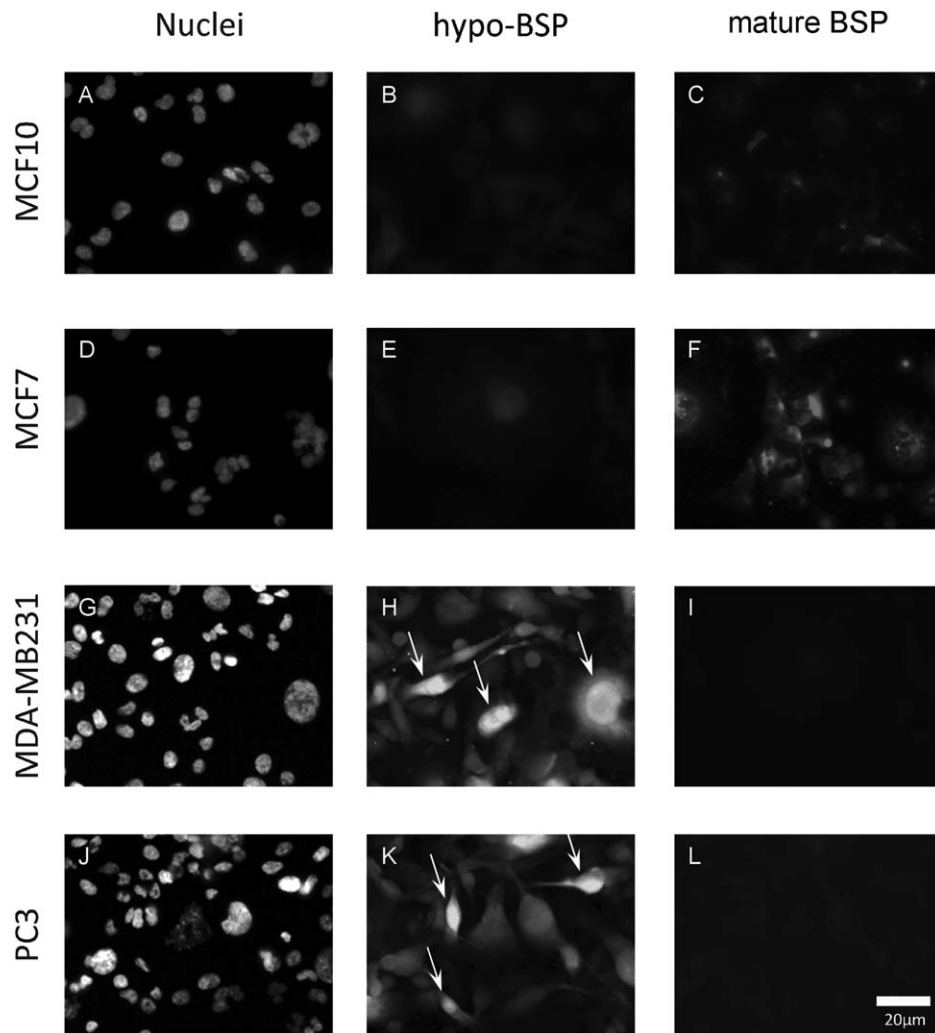


Figure 2. Double-fluorescence analysis of hypo-BSP and mature BSP. The non-cancer cell line MCF10 served as control and showed slight to moderate staining for BSP and traces of hypo-BSP (A–C). Hypo-BSP was low and mature BSP was slightly to moderately expressed in non-metastatic MCF7 cells (D–F). In contrast, metastasizing breast (MDA-MB-231; G–I) and prostate (PC3; J–L) cancer cells showed intensive staining of hypo-BSP (arrows), but only little staining for mature BSP. All images were taken at identical microscopic parameters and processed equally.

Immundiagnostik, Bensheim, Germany) by flow cytometry in MDA-MB-231, SaOS-2, and SK-OV-3 tumour cells. All cells expressed both forms of BSP intra-cellularly at low levels, but at their surface BSP expression was seen only for SK-OV-3 cells (supplementary material, Figure S2B).

Immunocytochemistry

Detection of BSP-forms in a panel of tumour cell lines. Cells of the immortal but non-tumourigenic MCF-10 line and those of the tumourigenic but not metastatic MCF-7 line were small or medium sized. No expression of cfH or integrin $\alpha_v\beta_3$ was detected (data not shown). In addition, traces of hypo-BSP

and slight to moderate expression of mature BSP were detected (Figure 2A–F). The morphology of MDA-MB-231 and PC3 cells varied strongly from small, mono-nuclear cells to mono- or poly-nuclear cells with abundant cytoplasm. Increased expression of all investigated antigens could be found in a fraction of cells derived from both cell lines. The expression pattern of mature BSP and hypo-BSP was inversely related to that of the non-metastatic cells (Figure 2G–L). At higher magnification, the level of mature BSP was higher in small- and medium-sized cells, both intra- and extra-cellularly, when comparing their status to that of the non-metastatic cells. Hypo-BSP could be found in large metastatic cells. Small metastatic cells did not express hypo-BSP;

medium-sized cells showed various patterns of both, hypo-BSP and mature BSP expression. In large cells, hypo-BSP was always accompanied by mature BSP, mainly located extra-cellularly. In special cases, hypo-BSP was detected in the nucleus. In these cases, mature BSP was only detectable extra-cellularly. The distribution pattern of both mature BSP (intra-cellular and extra-cellular) and hypo-BSP (no LSM evidence for extra-cellular distribution) was identical for MDA-MB-231 and PC3 cells (Figure 2G–L).

These observations were confirmed by results from the confocal laser scanning microscope, which was used for detecting the expression of mature BSP and hypo-BSP in MDA-MB-231 and PC3 cells (Figure 3A–D). For multiple staining, the green colour in the micrographs indicates hypo-BSP expression, whereas the presence of mature BSP, cfH, and integrin $\alpha_v\beta_3$ was visualized by red colour, respectively. Cell nuclei are shown by blue fluorescence.

Nearly all of the stained cells expressed cfH and integrin $\alpha_v\beta_3$ (Figure 3A,B). Completely green tinted cells (indicating hypo-BSP) showed smaller amounts of cfH, indicated by a yellow-orange colour (Figure 3A). The expression of integrin $\alpha_v\beta_3$ was comparable to that of cfH, as the expression was present in all cells. In the large hypo-BSP expressing cells, the co-localization of $\alpha_v\beta_3$ and hypo-BSP is indicated by yellow-orange colour (Figure 3B). It seems that smaller cells contained more red colour, indicating the presence of cfH and integrin $\alpha_v\beta_3$ without hypo-BSP. Concomitant expression of mature (red) and hypo-BSP was examined in PC3 (Figure 3C) and MDA-MB-231 (Figure 3D) cells. Within the cell populations, the expression pattern varied, as not all cells showed double staining. In cells showing red and green stains, there was only partial co-localization (orange colour). In many of the positive cells, hypo-BSP was present within the nucleus, whereas mature BSP was restricted to the perinuclear region, sparing the nucleus. Three-dimensional visualization of BSP expression was performed in MDA-MB-231 cells only (Figure 3E–G). Mature BSP showed a patchy distribution mainly on the cell surface, but hypo-BSP showed a granular distribution in the cytoplasm and the nucleus.

Detection of BSP-forms in osteoblasts and osteoclasts. In addition, the presence of BSP forms was analysed by immunocytochemistry in human osteoclasts (Figure 3H,I) and osteoblasts growing in the presence of collagen I (Figure 3J,K; collagen indicated by red colour). In both skeletal cell types, the cytosol stained positive for mature BSP, which is shown by green fluorescence (Figure 3H,J) but was negative for hypo-BSP (Figure 3I,K).

Detection of BSP-forms by immunohistochemistry

The two monoclonal antibodies were also compared for their staining patterns in samples obtained from lesions growing in nude rats following either subcutaneous or intra-arterial (femoral artery) injection of MDA-MB-231^{GFP/Luc} cells. In contrast to cell culture conditions, mature BSP was detected by the mouse monoclonal antibody (A4232.2) to be abundantly expressed in and around MDA-MB-231^{GFP/Luc} cells growing subcutaneously (Figure 4A1,A2) and as soft tumour around the femur (Figure 4B1,B2). Extraordinary intra-cellular production was also associated with vesicles filled with BSP, which were found in the extra-cellular space.

Compared to the mouse monoclonal antibody, the rat monoclonal antibody IDK-1 stained the tumour growing subcutaneously much less intensely (Figure 4C1,C2), but soft tumour tissue in the vicinity of the skeleton with similar intensity (Figure 4D1,D2). Notably, hypo-BSP was also stained intensely in necrotic areas of tumours growing *in vivo* (supplementary material, Figure S5). IDK-1 staining indicated distinct granular expression of hypo-BSP.

In addition to human breast cancer cells growing in nude rats, IDK-1 was also used for staining the primary tumour and respective skeletal metastases of 11 breast cancer patients. When assessing the IDK-1 staining intensity by a semi-quantitative score, primary lesions had an average score of 4.5 indicating hypo-BSP expression, but skeletal lesions had an average score of 8.3. This increase was highly significant when comparing the scoring results by the Wilcoxon rank sum test ($p < 0.004$). Tumour and metastasis samples from two breast cancer patients are shown in Figure 5. The photographs shown in Figure 5A–D are taken from a 45-year-old patient with a grade 2. The level of hypo-BSP increased from moderate local expression in the primary tumour (Figure 5B) to diffusely distributed moderate cytoplasmic expression in the corresponding metastasis (Figure 5D). The photographs in Figure 5E–H are taken from a 47-year-old patient with ductal breast cancer. Here, the hypo-BSP level increased from focal, moderate cytoplasmic expression (Figure 5F) to diffuse distribution of moderate to strong cytoplasmic expression (Figure 5H). An overview of eleven breast cancer patients with their grades and receptor status as well as a score describing the staining intensity of BSP in the primary cancer versus metastatic skeletal lesions is given in supplementary material, Table S2. The score intensity was significantly higher in metastatic than in primary lesions ($p < 0.004$).

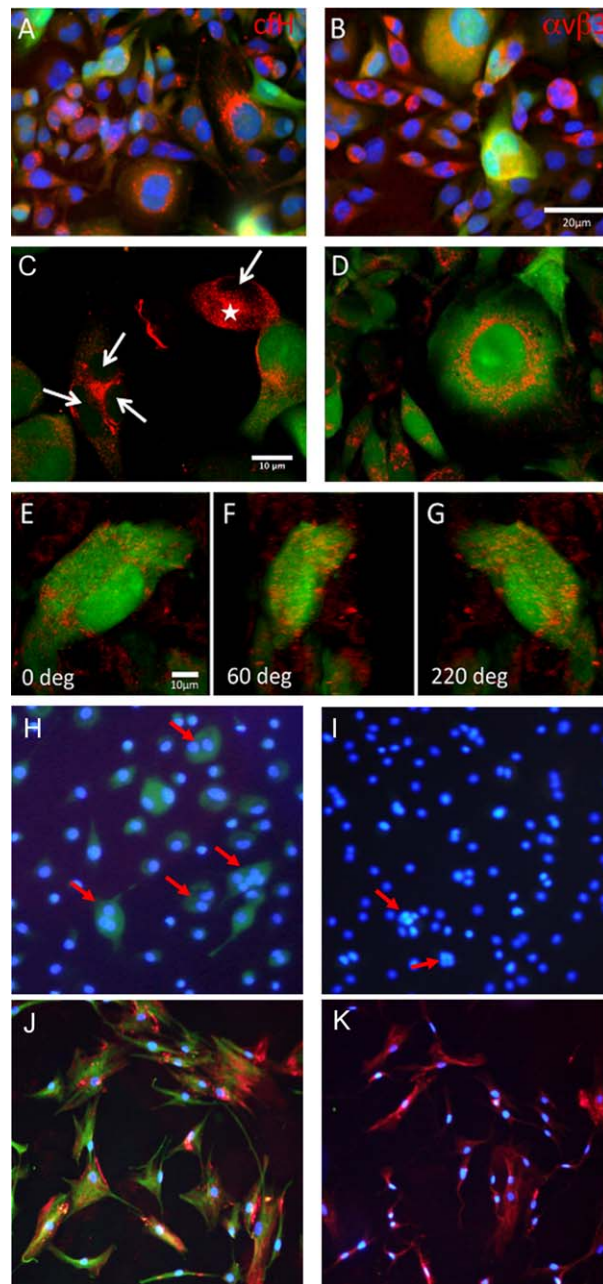


Figure 3. Co-localization of hypo-BSP and mature BSP as well as with possible interaction partners. Co-localization of hypoglycosylated BSP (hypo-BSP) (visualized with FITC; green colour) with (A) complement factor H (cfH) or (B) the vitronectin receptor ($\alpha_v\beta_3$) (visualized with TRITC; red colour) in MDA-MB-231 cells. (C, D) Confocal laser scanning analysis of PC3 and MDA-MB-231 cells. Mature BSP (red) and hypo-BSP (green) show only partial co-localization (orange colour). In many cells, hypo-BSP was also observed within the nucleus, while mature BSP was clearly restricted to the perinuclear region, sparing the nucleus (arrows in C). The expression pattern varied within the cell population, i.e. not all of the cells showed hypo-BSP and mature BSP double-staining (asterisk in C). Laser scanning features demonstrate the similarities in the PC3 and MDA-MB-231 cells. (E–G) Three-dimensional visualization of a 36 image stack obtained by laser scanning microscopy of a MDA-MB-231 cell. Note the patchy distribution of mature BSP (red) mainly on the cell surface, while hypo-BSP (green) shows granular distribution in the cytoplasm and the kidney-shaped nucleus. (H–K) Detection of mature BSP and hypo-BSP in human osteoclasts (H, I: red arrows) and osteoblasts growing in the presence of collagen I (J, K: collagen indicated by red colour). In both skeletal cell types the cytosol stained positive for mature BSP, which is shown by green fluorescence (H, J) but was negative for hypo-BSP (I, K).

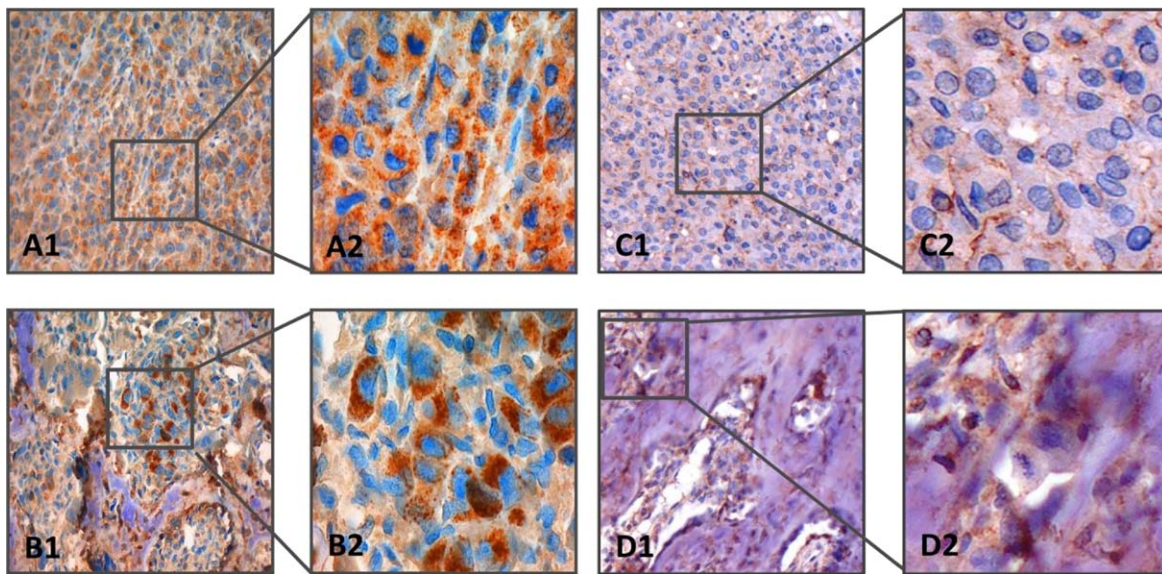


Figure 4. Immunostaining of MDA-MB-231 breast cancer cell-derived tumours. Mature BSP was stained with mouse monoclonal antibody A4232.2. The upper row (A1, A2) shows a tumour growing subcutaneously (left image: $\times 20$ objective magnification, right image: $\times 63$ objective magnification). The lower row (B1, B2) shows tumour growing adjacent to rat femur (left image: $\times 20$ objective magnification, right image: $\times 63$ objective magnification). Nuclei are stained blue; BSP is indicated by brown colour. Distinct granular cytoplasmic expression of mature BSP is found under both conditions. At higher magnification, vesicles filled with mature BSP are found in the extra-cellular space. Hypoglycosylated BSP was stained with rat monoclonal antibody IDK-1. The upper row (C1, C2) shows a tumour growing subcutaneously (left image: $\times 20$ objective magnification, right image: $\times 63$ objective magnification). The lower row (D1, D2) shows tumour growing adjacent to rat femur (left image: $\times 20$ objective magnification, right image: $\times 63$ objective magnification). Nuclei are stained blue; hypoglycosylated BSP is indicated by brown colour. Local diffuse cytoplasmic expression of hypoglycosylated BSP is found in tumours growing subcutaneously; in contrast, distinct granular expression of hypoglycosylated BSP is observed in tumour growing adjacent to bone tissue.

Specificity of IDK1

The specificity of IDK1 was assessed in whole cell lysates from MDA-MB-231 cells grown *in vitro* and *in vivo* (the latter isolated from a breast cancer skeletal metastasis growing in a nude rat). Immunoblotting for hypo-BSP showed a 3.6-fold increased level of BSP expression between cells growing *in vitro* and *in vivo*. Similarly, all three histone demethylases (histone lysine demethylase PHF8, lysine-specific demethylase 3B [KDM3B], and lysine-specific demethylase PHF2), which contain the IDK1 target sequence TGLAA, were detected with their specific antibodies, but not with IDK1, as there were no bands visible that showed a size similar to that of the demethylases (supplementary material, Figure S6).

Cross-reaction with murine BSP

To further characterize the specificity of IDK1, the femur of a mouse was stained with IDK1 for hypo-BSP. There was no staining of any structure, including osteoblasts and osteoclasts (data not shown).

Discussion

Post-translational modifications including glycosylation profiles can change significantly during oncogenesis [24] and represent a promising source for potential biomarkers [25]. For example, breast cancer patients can secrete MUC1 glycoprotein with *O*-linked oligosaccharides, which differs from that of healthy tissues [26] and this altered glycosylation is used for detecting breast cancer. The use of an altered glycosylation pattern as a biomarker for cancer diagnostics is only one example of a growing area [25]. Here, we add hypo-BSP to this list of markers and show concomitantly the potential of this glycoprotein as a target for treating skeletal metastasis.

The monoclonal rat antibody IDK1 showed good affinity for hypo-BSP, but none for mature BSP and induced higher rates of complete remission in nude rats harbouring MDA-MB-231-induced skeletal lesions than a polyclonal IgY antibody against BSP that was used previously [27]. In contrast to the IgY antibody, IDK1 was not cytotoxic *in vitro*. This

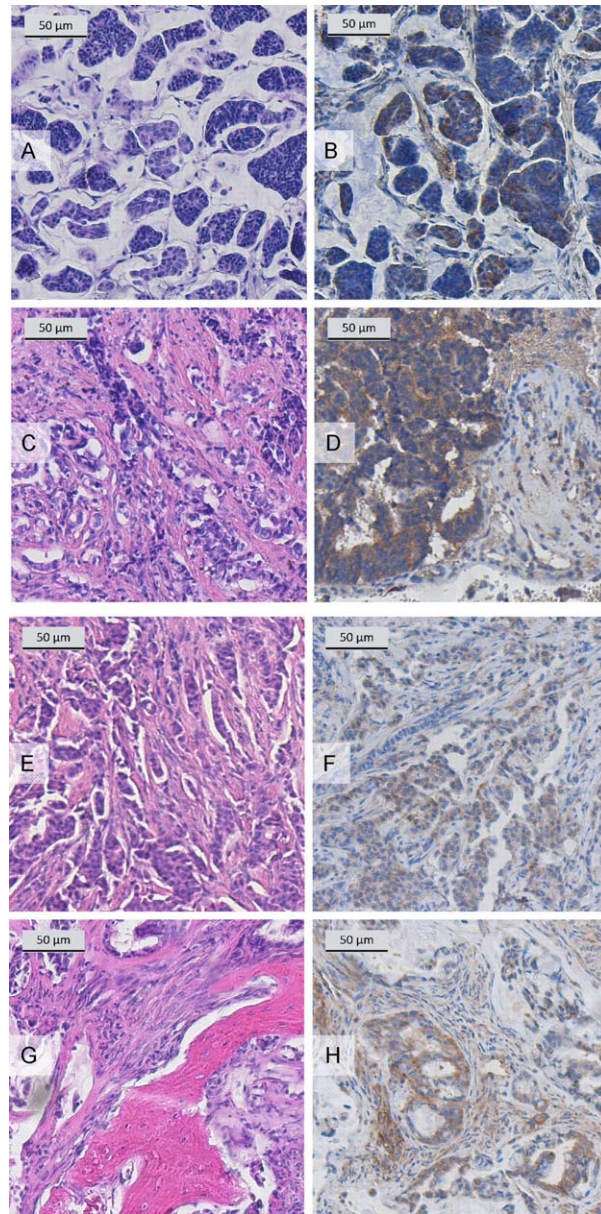


Figure 5. Immunostaining of specimens from breast cancer patients. Mucinous, grade 2 breast cancer of a 45-year-old female patient (ER positive, PR weakly positive, Her2 negative; (A) HE stain of the primary carcinoma ($\times 10$ objective magnification); (B) hypo-BSP stain of the primary carcinoma with rat monoclonal antibody IDK-1 ($\times 20$ objective magnification) showing moderate local expression; (C) HE stain of metachronous (7 years) spinal metastasis (thoracic vertebrae 3 + 4, $\times 4$ objective magnification); (D) hypo-BSP stain of a metachronous (7 years) spinal metastasis with rat monoclonal antibody IDK1 ($\times 40$ magnification) showing diffuse distribution of moderate cytoplasmic hypo-BSP expression. Invasive, grade 2 ductal breast cancer of a 47-year-old female patient (ER strongly positive, PR strongly positive, Her2 negative; (E) HE stain of the primary carcinoma ($\times 4$ objective magnification); (F) hypoglycosylated BSP stain of the primary carcinoma with rat monoclonal antibody IDK1 ($\times 4$ objective magnification) showing focal, moderate cytoplasmic expression; (G) HE stain of a synchronous spinal metastasis (thoracic vertebra 6, $\times 20$ objective magnification); (H) hypoglycosylated BSP stain of a synchronous spinal metastasis with rat monoclonal antibody IDK1 ($\times 20$ objective magnification) showing diffuse distribution of moderate to strong cytoplasmic expression.

observation and the finding that MDA-MB-231 cells secrete large amounts of both BSP forms only *in vivo* shed some light on the putative mechanism of action of IDK1. We assume that hypo-BSP, which was

preferentially produced in the vicinity of the rat skeleton, is involved in the formation of lytic skeletal lesions. The capture of hypo-BSP by IDK1, similar to a decoy receptor, may then have decreased this

effect. This hypothesis does not exclude that complexes of IDK1 and hypo-BSP are located on the membrane of tumour cells and induced complement activation, which has been described in nude rats [28]. This reaction could be initiated by binding of BSP to integrin $\alpha_v\beta_3$, which is amply present on MDA-MB-231 cells (Figure 3B). Based on this, integrin $\alpha_v\beta_3$ has been successfully targeted by its inhibitor cilengitide and this treatment correlated with significant growth inhibition of MDA-MB-231 skeletal metastases [29]. Despite the presence of $\alpha_v\beta_3$, our FACS analyses showed no BSP on the surface of MDA-MB-231 cells growing in cell culture. Although this could be different *in vivo* because of the increased expression of BSP, the lack of any anti-proliferative activity of IDK1, even in experiments using FBS without heat inactivation, lowers the probability that complement activation is a decisive factor in the mechanism of action of IDK1. Moreover, the abundant presence of cfH on MDA-MB-231 cells (Figure 3A) could be interpreted as part of their immune evasion strategy [30] and further add to the lack of complement activation.

The expression of mature and hypo-BSP in cells growing *in vitro* was low, even in the metastatic cell line MDA-MB-231. However, when comparing selected cells positive for BSP, there was more expression of hypo-BSP in the metastatic cell lines MDA-MB-231 and PC3 than in non-metastatic or non-malignant cells. One typical but puzzling site of hypo-BSP was the nucleus, whereas mature BSP was mainly prevalent in the perinuclear region. There was also co-expression and partial co-localization with cfH and integrin $\alpha_v\beta_3$, which are potential interaction partners [31]. However, the main sites of BSP expression *in vivo* were cytoplasm and membranes. Nuclei were partially condensed, thus giving rise to assumed low BSP concentrations, but there was no conclusive evidence. The following reasons, nevertheless, might indicate a role of BSP in the nucleus: conditional knockdown of BSP caused not only complete regression of established MDA-MB-231 skeletal lesions, but also intensive alterations of cellular signalling cascades and induction of apoptosis [20]. Finally, immunoblotting of nuclear extracts from tumour tissue growing in the vicinity of skeletal lesions showed a strong band indicative of hypo-BSP. This could imply a role of BSP that has not been unravelled so far. An alternative possibility is the presence of other proteins containing the TGLAA motif, including the histone demethylases PHF8, KDM3B, and PHF2, which are nuclear constituents. Thus, only future experiments will shed light on these open questions.

In the model used, the activity of IDK1, which induced complete remission in up to 80% of rats, is unsurpassed to the best of our knowledge by any other compound and may alter skeletal metastasis treatment if the results will translate into the clinical situation. The reason for this activity presumably is a change in BSP expression of MDA-MB-231 cells under *in vivo* conditions. The poor expression of BSP *in vitro* is dramatically increased *in vivo*, regardless of the site of implantation (Figure 4). The specificity of IDK1 results, however, from differential expression of hypo-BSP in primary and metastatic sites: MDA-MB-231^{GFP/Luc} tumours growing subcutaneously express large amounts of mature BSP, but only few hypo-BSP. In concordance with this observation, IDK1 has little activity in MDA-MB-231^{GFP/Luc} tumours growing subcutaneously, but impressive activity at skeletal site lesions, which are characterized by large amounts of hypo-BSP. These observations are related to the human pathology, as tissues from skeletal metastases expressed significantly more hypo-BSP than those from the respective primary breast cancers. Notwithstanding this congruency of animal model and human pathologies, some caveats are needed for interpreting the results. The use of a T-cell deficient model for screening immunotherapeutic agents has restrictions as these models are not applicable for studying checkpoint blockers [32]. However, the use of syngeneic mouse models was excluded due to the lack of IDK1 cross-reactivity with mouse BSP (unpublished own data) and, likewise, the use of humanized models was precluded by their availability. It should be kept in mind, however, that the putative mechanism of action does not include the activity of T-cells and that using IDK1 for capturing hypo-BSP has analogies to using denosumab as a decoy receptor of RANKL [33,34]. Another aspect of the model is that side effects on the skeleton cannot be predicted sufficiently because of the species differences in BSP composition. Our initial results suggest no interaction of IDK1 with human osteoblasts and osteoclasts, but future experiments will have to elucidate any toxic effect of IDK1 on human bone physiology.

In conclusion, hypo-BSP is a promising biomarker of skeletal metastasis, which can be used for diagnostic purposes. After transforming this monoclonal rat antibody into a human version, it can also be tested for its potential application in patients. If the encouraging results of this study translate into clinical application, a new treatment option for skeletal metastases will be available. Such studies are highly warranted.

Acknowledgement

This study was supported by a grant from the Federal Ministry for Education and Research (# 0315855).

Author contributions statement

FPA, MRB: designed the study; MZ, MK, MA, KF, HH, JN, GMH: collected data; MZ, GW, IB, HH, MRB: analyzed data; MZ: searched for literature; MZ, HH, JN, MRB: generated figures; IB, MRB: interpreted data; MZ, GW, HH, MRB: wrote the manuscript. All authors added to writing the paper and had final approval of the submitted and published versions.

References

- Cornelissen LA, Van Vliet SJ. A bitter sweet symphony: immune responses to altered O-glycan epitopes in cancer. *Biomolecules* 2016; **6**: 26.
- Pinho SS, Reis CA. Glycosylation in cancer: mechanisms and clinical implications. *Nat Rev Cancer* 2015; **15**: 540–555.
- Wuttke M, Müller S, Nitsche DP, et al. Structural characterization of human recombinant and bone-derived bone sialoprotein. Functional implications for cell attachment and hydroxyapatite binding. *J Biol Chem* 2001; **276**: 36839–36848.
- Bellahcène A, Castronovo V, Ogbureke KUE, et al. Small integrin-binding ligand N-linked glycoproteins (SIBLINGs): multi-functional proteins in cancer. *Nat Rev Cancer* 2008; **8**: 212–226.
- Uccello M, Malaguarnera G, Vacante M, et al. Serum bone sialoprotein levels and bone metastases. *J Cancer Res Ther* 2011; **7**: 115–119.
- Ruoslahti E. RGD and other recognition sequences for integrins. *Annu Rev Cell Dev Biol* 1996; **12**: 697–715.
- Ruoslahti E. Integrin signaling and matrix assembly. *Tumour Biol* 1996; **17**: 117–124.
- Bellahcène A, Menard S, Bufalino R, et al. Expression of bone sialoprotein in primary human breast cancer is associated with poor survival. *Int J Cancer* 1996; **69**: 350–353.
- Diel IJ, Solomayer EF, Seibel MJ, et al. Serum bone sialoprotein in patients with primary breast cancer is a prognostic marker for subsequent bone metastasis. *Clin Cancer Res* 1999; **5**: 3914–3919.
- Gillespie MT, Thomas RJ, Pu Z-Y, et al. Calcitonin receptors, bone sialoprotein and osteopontin are expressed in primary breast cancers. *Int J Cancer* 1997; **73**: 812–815.
- Waltregny D, Bellahcène A, Castronovo V, et al. Prognostic value of bone sialoprotein expression in clinically localized human prostate cancer. *J Natl Cancer Inst* 1998; **90**: 1000–1008.
- Bellahcène A, Albert V, Pollina L, et al. Ectopic expression of bone sialoprotein in human thyroid cancer. *Thyroid* 1998; **8**: 637–641.
- Adwan H, Bauerle TJ, Berger MR. Downregulation of osteopontin and bone sialoprotein II is related to reduced colony formation and metastasis formation of MDA-MB-231 human breast cancer cells. *Cancer Gene Ther* 2004; **11**: 109–120.
- Adwan H, Bauerle T, Najajreh Y, et al. Decreased levels of osteopontin and bone sialoprotein II are correlated with reduced proliferation, colony formation, and migration of GFP-MDA-MB-231 cells. *Int J Oncol* 2004; **24**: 1235–1244.
- Fedarko NS, Fohr B, Robey PG, et al. Factor H binding to bone sialoprotein and osteopontin enables tumor cell evasion of complement-mediated attack. *J Biol Chem* 2000; **275**: 16666–16672.
- Karadag A, Fisher LW. Bone sialoprotein enhances migration of bone marrow stromal cells through matrices by bridging MMP-2 to alpha(v)beta3-integrin. *J Bone Miner Res* 2006; **21**: 1627–1636.
- Dapunt U, Giese T, Maurer S, et al. Neutrophil-derived MRP-14 is up-regulated in infectious osteomyelitis and stimulates osteoclast generation. *J Leukoc Biol* 2015; **98**: 575–582.
- Reufsteck C, Lifshitz-Shovali R, Zepp M, et al. Silencing of skeletal metastasis-associated genes impairs migration of breast cancer cells and reduces osteolytic bone lesions. *Clin Exp Metastasis* 2012; **29**: 441–456.
- Pervaiz A, Ansari S, Berger MR, et al. CCR5 blockage by maraviroc induces cytotoxic and apoptotic effects in colorectal cancer cells. *Med Oncol* 2015; **32**: 158.
- Kovacheva M, Zepp M, Berger SM, et al. Sustained conditional knockdown reveals intracellular bone sialoprotein as essential for breast cancer skeletal metastasis. *Oncotarget* 2014; **5**: 5510–5522.
- Zepp M, Bäuerle TJ, Elazar V, et al. Treatment of breast cancer lytic skeletal metastasis using a model in nude rats. In *Breast Cancer - Current and Alternative Therapeutic Modalities*, Gunduz E, Gunduz M (Eds). InTech Open Access Publisher: Rijeka, Croatia, 2012; 453–488.
- Bäuerle T, Hilbig H, Bartling S, et al. Bevacizumab inhibits breast cancer-induced osteolysis, surrounding soft tissue metastasis, and angiogenesis in rats as visualized by VCT and MRI. *Neoplasia* 2008; **10**: 511–520.
- Fortunato F, Berger I, Gross M-L, et al. Immune-compromised state in the rat pancreas after chronic alcohol exposure: the role of peroxisome proliferator-activated receptor gamma. *J Pathol* 2007; **213**: 441–452.
- Kailemia MJ, Park D, Lebrilla CB. Glycans and glycoproteins as specific biomarkers for cancer. *Anal Bioanal Chem* 2017; **409**: 395–410.
- Kirwan A, Utratna M, O'Dwyer ME, et al. Glycosylation-based serum biomarkers for cancer diagnostics and prognostics. *Biomed Res Int* 2015; **2015**: 490531.
- Mukhopadhyay P, Chakraborty S, Ponnusamy MP, et al. Mucins in the pathogenesis of breast cancer: implications in diagnosis, prognosis and therapy. *Biochim Biophys Acta* 2011; **1815**: 224–240.
- Bäuerle T, Adwan H, Kiessling F, et al. Characterization of a rat model with site-specific bone metastasis induced by MDA-MB-231 breast cancer cells and its application to the effects of an antibody against bone sialoprotein. *Int J Cancer* 2005; **115**: 177–186.
- Chen S, Caragine T, Cheung NK, et al. CD59 expressed on a tumor cell surface modulates decay-accelerating factor expression and enhances tumor growth in a rat model of human neuroblastoma. *Cancer Res* 2000; **60**: 3013–3018.
- Bäuerle T, Komljenovic D, Merz M, et al. Cilengitide inhibits progression of experimental breast cancer bone metastases as

- imaged noninvasively using VCT, MRI and DCE-MRI in a longitudinal in vivo study. *Int J Cancer* 2011; **128**: 2453–2462.
30. Parente R, Clark SJ, Inforzato A, et al. Complement factor H in host defense and immune evasion. *Cell Mol Life Sci* 2017; **74**: 1605–1624.
 31. Kruger TE, Miller AH, Godwin AK, et al. Bone sialoprotein and osteopontin in bone metastasis of osteotropic cancers. *Crit Rev Oncol Hematol* 2014; **89**: 330–341.
 32. Sanmamed MF, Chester C, Melero I, et al. Defining the optimal murine models to investigate immune checkpoint blockers and their combination with other immunotherapies. *Ann Oncol* 2016; **27**: 1190–1198.
 33. Schieferdecker A, Voigt M, Riecken K, et al. Denosumab mimics the natural decoy receptor osteoprotegerin by interacting with its major binding site on RANKL. *Oncotarget* 2014; **5**: 6647–6653.
 34. Lipton A, Fizazi K, Stopeck AT, et al. Effect of denosumab versus zoledronic acid in preventing skeletal-related events in patients with bone metastases by baseline characteristics. *Eur J Cancer* 2016; **53**: 75–83.

SUPPLEMENTARY MATERIAL ONLINE

Supplementary materials and methods

Supplementary figure legends

Figure S1. Affinity of antibodies to bone sialoprotein forms

Figure S2. Flow cytometry analysis

Figure S3. Growth of MDA-MB-231-induced skeletal lesions in nude rats: comparison of imaging methods

Figure S4. Histological evaluation of rat hind legs after treatment with IDK-1

Figure S5. Immunohistochemical staining of a partially necrotic MDA-MB-231 tumour for hypo-glycosylated bone sialoprotein

Figure S6. Hypoglycosylated BSP, histone lysine demethylase PHF8, lysine-specific demethylase 3B (KDM3B), and lysine-specific demethylase PHF2 in whole cell lysates from MDA-MB-231 cells *in vitro* and *in vivo*

Table S1. Experimental set up and results from testing three monoclonal antibodies against hypo-BSP for anti-proliferative and anti-migratory effects

Table S2. Evaluation of hypo-BSP staining intensity by semi-quantitative scoring in 11 paired human samples